# Defect-Tolerant Single-Electron Charging at Room Temperature in Metal Nanoparticle Decorated Biopolymers**

By *Christopher A. Berven*, *Laura Clarke*, *Jana L. Mooster*, *Martin N. Wybourne*,* and *James E. Hutchison*

The last three decades have seen a dramatic decrease in the size of microelectronic devices, with the number of devices on a microchip doubling about every eighteen months.[1] As device feature sizes shrink towards quantum scales, this evolution is facing serious technical, fundamental, and economic challenges. To address these issues a number of revolutionary departures from the conventional semiconductor device paradigm are currently being investigated. In particular, nanostructures, in which single electron tunneling and charging effects can be exploited for device applications, (e.g., in quantum cellular automata[2] and organic thin-film transistors[3]) are receiving much attention.

The effects of single-electron charging on electron transport in lithographically-defined nanostructures is well-documented.[4] In general, nanostructures at the limits of electron-beam lithography (ca. 15 nm) are too large to achieve clear single-electron effects at room temperature. Alternative approaches to achieve these effects at room temperature include silicon nanocrystal floating gate devices[5] and focused ion beam deposited structures.[6] Another involves assemblies of metal or semiconductor nanoparticles that have well-defined dimensions down to the molecular scale. At these sizes the inherent capacitance of the system is small enough that single-electron effects are manifest at room temperature. An added advantage is that the chemical nature of these building blocks makes possible the parallel chemical assembly of particle arrays from individual particles with precisely tuned physical properties.

In order to utilize nanoparticle building blocks, or even to explore their electrical properties, it is important to be able to assemble and make electrical contact to them. Considerable progress has been made toward the rational assembly of extended nanoparticle arrays,[7,8] and transport measurements perpendicular to the plane of the arrays have been performed using scanning probe microscopy and thin film electrode sandwich arrangements.[9–11] Measurements that probe lateral transport (in the plane of the array) in two-dimensional films and patterned arrays such as lines are important for designing planar device applications. Given the finite yield of the chemical assembly process, defects will exist in these arrays and might be expected to adversely influence the transport properties. Although the importance of defect tolerance in chemically-assembled nanoscale electronic circuits has been discussed in the context of other systems,[12,13] the potential of near room temperature experiments on patterned nanoparticle arrays[14–18] to probe the defect- and disorder-sensitivity remains largely unexplored.

Here we present the room-temperature electrical behavior of gold nanoparticles assembled on a biopolymer template deposited between metal electrodes on an insulating substrate. The assemblies were prepared using a straightforward procedure that involves only wet chemical methods. Unambiguous single-electron charging effects are observed that can be understood in terms of the nanoparticle properties and the geometrical constraints imposed by the biopolymer. These results support the idea of using nanoparticles in conjunction with biomolecular organization to achieve nanoscale systems with novel, defect-tolerant current–voltage behavior.

Networks of gold nanoparticles were fabricated between the fingers of gold interdigitated array (IDA) electrodes (15 or 2 μm gap) by electrostatic assembly of carboxylic acid modified gold nanoparticles onto the amino side chains of the biopolymer poly-L-lysine (PLL).[19] A thin film of PLL (MW = 54 000 amu) is initially deposited from aqueous methanol containing the alpha-helical form of its hydrobromide salt. The exposed side chains of the dried film were subsequently deprotonated by soaking in dilute base. The 11-mercaptoundecanoic acid-stabilized gold nanoparticles were assembled onto the biopolymer from an organic solvent. The metal-core radius was determined to be 0.7 ± 0.2 nm (±30 %) by transmission electron microscopy (TEM), and the diameter of the core and ligand shell together is estimated to be 4.2 nm. The average length of an extended PLL chain is ca. 30 nm.

Current–voltage (*I–V*) measurements were performed at room temperature with the samples in an electrically shielded vacuum chamber.[20] Control measurements were made on the bare electrodes and again after the PLL had been deposited and deprotonated. The *I–V* characteristics of the deprotonated PLL and the bare surface were linear (ohmic) without any structure, as shown by curve I in Figure 1a. Importantly, these two sets of control data were indistinguishable, which shows that to within experimental uncertainty the surface conductance of the glass substrate was unaffected by the deprotonated PLL. In contrast, when decorated with nanoparticles, the samples exhibited pronounced nonlinear *I–V* characteristics, as shown by curve II in Figure 1a. After subtraction of the linear *I–V* behavior measured before PLL decoration, to within the measurement accuracy the electrical characteristics showed a region of zero conductance at low voltages. The onset of current is characterized by a threshold voltage, $V_T$,

[*] Prof. M. N. Wybourne, Dr. C. A. Berven, Dr. L. Clarke[+]
Department of Physics and Astronomy
Dartmouth College
Hanover, NH 03755 (USA)
E-mail: martin.n.wynbourne@dartmouth.edu
J. L. Mooster, Prof. J. E. Hutchison
Department of Chemistry
University of Oregon
Eugene, OR 97403 (USA)
[+] Present address: Department of Physics, University of Colorado at Boulder, Boulder, CO, USA.

[**] This work was supported in part by the Office of Naval Research, the National Science Foundation (DMR-9705343) and the Camille and Henry Dreyfus Foundation. JEH is an Alfred P. Sloan Research Fellow. We are grateful to Dr. Masao Morita of NTT (Japan) for supplying the 2 μm IDA electrodes used in this work.

  0935-9648/01/0201-0109 $ 17.50+.50/0 

ADVANCED MATERIALS

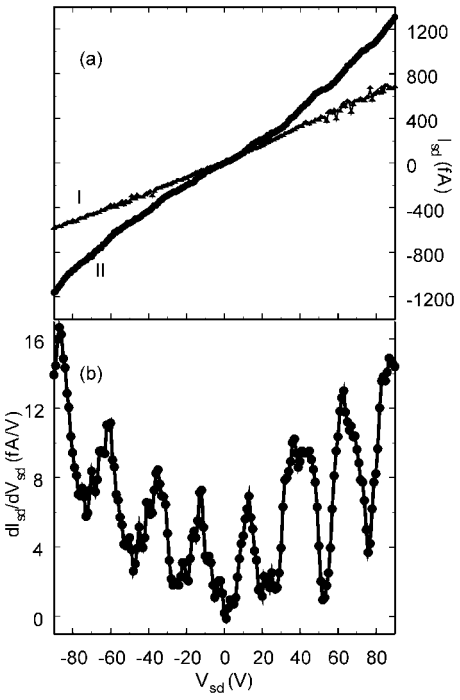


Fig. 1. a) The *I–V* characteristics of the PLL film after deprotonation (curve I) and after decoration with the gold nanoparticles (curve II). b) The conductance of the PLL gold nanoparticle system. All measurements were made at 300 K.

that was found to be different for different samples. Above the threshold, the current increases and the scaling $I \propto (V/V_T - 1)^{\gamma}$ was found to describe all sets of data with $\gamma = 1.2 \pm 0.2$. Here the error includes the uncertainty in the current measurement and the spread between different data sets. At voltages above threshold, structure of period $\Delta V$ was observed in the *I–V* curves of most samples, with the ratio $\Delta V/V_T \approx 2$. This is most easily seen in the conductance, as shown in Figure 1b. For this data the measured threshold voltage is $V_T = 12 \pm 1$ V, and the period of the oscillations is $\Delta V = 25 \pm 3$ V.

The value of the scaling exponent $\gamma$ is indicative of the electronic degrees of freedom in the sample. The values obtained for our samples are consistent with single-electron transport in one-dimensional systems where it is predicted that $\gamma \approx 1$.[21,22] These predictions are supported by measurements of the low-temperature transport in one-dimensional chains of lithographically-defined tunnel junctions that found $\gamma = 1.36 \pm 0.1$.[23] Further, the almost linear scaling is distinct from the quadratic scaling reported for thin films containing gold nanoparticles.[24] The current–voltage scaling, threshold behavior and periodic structure are all reminiscent of single-electron behavior in one-dimensional systems, with the region of zero conductance resulting from a Coulomb gap at the Fermi level. These are remarkable results given the simple method of sample fabrication and the fact that the measurements were made at 300 K. One intriguing feature is the voltage scale of the conductance structure, which is considerably larger than commonly found in other single electron systems.

To study the morphology of the hybrid nanoparticle/PLL assemblies, samples were prepared on mica under the identical conditions to those used to make the samples for the electrical measurements. The assemblies were imaged using tapping mode atomic force microscopy (AFM). The initial, dried PLL·HBr films were found to be smooth with voids probably due to film contraction while drying. During the deprotonation step, PLL is removed and the film becomes more porous, leading to a sub-monolayer lattice of PLL aggregate as shown in Figure 2a. Eventually, as more PLL is removed, the film becomes undetectable by AFM. However, upon decoration

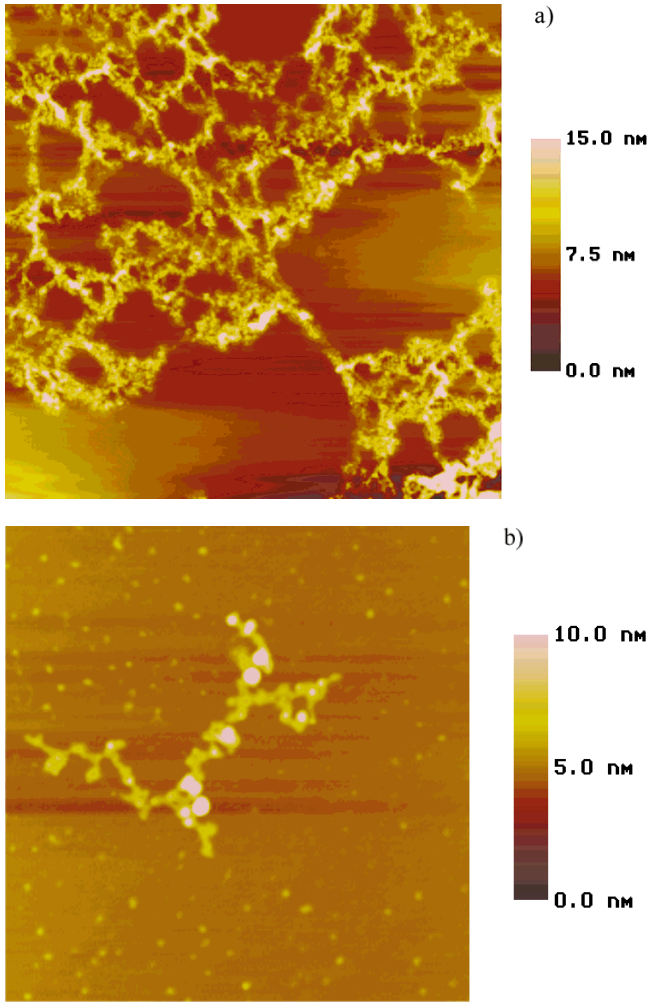


Fig. 2. Tapping mode AFM images. a) A typical 5.0 × 5.0 μm area showing PLL aggregates on mica as a result of soaking a thin PLL film in dilute sodium hydroxide for 20 h. b) A typical 1.2 × 1.2 μm area showing mercaptoundecanoic acid-stabilized gold nanoparticle arrays formed on mica substrates previously treated with PLL hydrobromide salt and soaked in dilute sodium hydroxide until the PLL was no longer detectable. The individual "dots" away from the main structure are isolated nanoparticles.

with functionalized nanoparticles, extended, chain-like assemblies are observed, as shown in Figure 2b. These experiments show that our wet chemical fabrication method is capable of producing quasi one-dimensional structures, consistent with the morphology suggested by the current scaling above threshold. The surface coverage of these structures is low, far below that required for a continuous path to be formed between the electrodes. This observation rules out the possi-

  0935-9648/01/0201-0110 $ 17.50+.50/0 

bility that bottleneck regions, or a single pathway dominate the electrical behavior. Individual nanoparticles are also found on the surface after chemical fabrication. Their low areal density, see Figure 2b, gives an average separation considerably larger than the distance between the nanoparticles forming the extended chains. Thus, the isolated nanoparticles are unlikely to contribute to the overall electrical behavior.

The electrical properties suggest single electron effects in one-dimensional structures and the AFM images show that the fabrication method is capable of producing such structures. However, there is an apparent discrepancy between the disordered nature of the sample seen by AFM (a collection of randomly sized, placed, and oriented nanoparticle arrays) and the clearly defined, periodic conductance features in the electrical characteristics that suggest an ordered system. To address this issue, as well as the voltage scale of the *I–V* structure, we have computed the electrical behavior of randomly oriented nanoparticle arrays that contain defects. We find that periodic conductance features occur despite the presence of defects and that surface conduction in conjunction with conduction through the array can explain the large voltage scale found in the data.

Single-electron charging effects are governed by the capacitance between adjacent nanoparticles and the capacitance of each nanoparticle to a ground plane. We treat the nanoparticles as identical metal spheres of radius 0.7 nm surrounded by a homogeneous ligand shell with a dielectric constant of 3. Including the ligand shell, the minimum center-to-center separation is 4.2 nm. Calculating the capacitance matrix for a row of nanoparticles we find an inter-particle capacitance $C_{dd} \approx$ 0.04 aF and a capacitance to ground $C_g \approx 0.17$ aF.[25] Thus, the dimensions of these nanoparticle building blocks result in a regime where $C_g > C_{dd}$, which is opposite to that studied in most lithographically defined systems. The capacitance values imply that the total capacitance of a nanoparticle is dominated by $C_g$ and the calculated value shows that the electrostatic charging energy $e^2/2C_g$ is more than an order of magnitude larger than $k_BT$ at 300 K, consistent with Coulomb blockade effects at room temperature.

Numerical simulations[26] of perfect chains confirm that threshold behavior, linear scaling above threshold, and a Coulomb staircase can all be expected at room temperature. To simulate the number of conductance peaks we observe, a minimum of four particles is required in a chain. While the expected and experimental values of the ratio $\Delta V/V_T$ agree, there is a discrepancy in the absolute voltage values for the threshold and the periodicity. The anticipated value of $V_T \approx e/2C_g = 0.47$ V is more than a factor of twenty smaller than the measured value. Reducing $C_g$ will increase $V_T$. However, assuming that at very small dimensions the capacitance can still be estimated from the geometry of a particle, the reduction in $C_g$ necessary to explain the data would require nanoparticles with impossibly small radii. From this argument we conclude that the conduction path must include potential drops that may be the result of contact resistance between the electrodes and the nanoparticle system, surface conduction, weak links within the network itself, or a combination of all three. We will address this issue in the discussion of the nature of the conduction path.

Before we consider the realistic situation of less than perfect chains randomly oriented on the surface, we note that the presence of radio frequency (RF) signals and other phenomena, such as quantum size effects[27] and the physical motion of nanoparticles in a field (the shuttle mechanism)[28] can also introduce conductance features. RF signals applied to the sample[20] had no perceivable affect on the conductance structure. Quantum size effects are weak at room temperature and the energy level structure is highly dependent on the structure of the nanoparticles, the ligands and the coupling between particles.[29] Thus, it seems unlikely that resonant tunneling through discrete electronic levels is the cause of the regularly spaced structure we observe. We rule out a shuttle mechanism because it predicts structure equally spaced in current rather than in voltage as we find. For the *I–V* characteristics we measure, this mechanism would also require vibrational frequencies that are much lower than is reasonable for the properties of the ligand.

Given the preparation method and the large area (~3 mm$^2$) sampled by the IDA electrodes, disorder and spatial averaging are expected in the samples. The types of disorder expected to have the greatest influence on the electrical properties are variations in core size that influence $C_g$ and the particle–particle spacing (positional disorder) that affects $C_{dd}$. In addition, the effects of particle chain length and chain orientation must be considered. We used numerical simulations to explore these effects individually and in combination. Chains of between four and nine particles whose core radii were randomly dispersed by up to ±30 % (the measured value) showed conductance structure that was periodic to within the measurement uncertainty (±12 %). For chains that contain ten or more particles, the uncertainty in the periodicity was much larger than we measure. Similarly, when the radius dispersion was increased to ±50 % the position of the conductance peaks was found to change significantly and the ratio $\Delta V/V_T$ deviated markedly from a value of two. Dispersion in $C_{dd}$ due to a distribution of particle–particle spacings was found to have little effect on the features. This is not surprising for a system in which $C_g > C_{dd}$ since the conductance is relatively insensitive to the inter-particle capacitance. From this analysis we conclude that individual one-dimensional chains containing less than ten particles with ±30 % radius variation can support Coulomb staircase behavior.

When many chains are in parallel the periodicity is maintained provided the chain lengths have a narrow distribution, implying that the samples contain chains of a well-defined length. This length may arise from individual PLL chains that, based on their molecular weight, can accommodate seven or eight nanoparticles. Given length uniformity, angular averaging over all possible orientations of a perfect chain between the electrodes does not remove the conductance peaks, but does broaden them and increases the conductance in the valleys between peaks, as shown by the dashed curve in Figure 3.

  0935-9648/01/0201-0111 $ 17.50+.50/0 

ADVANCED MATERIALS

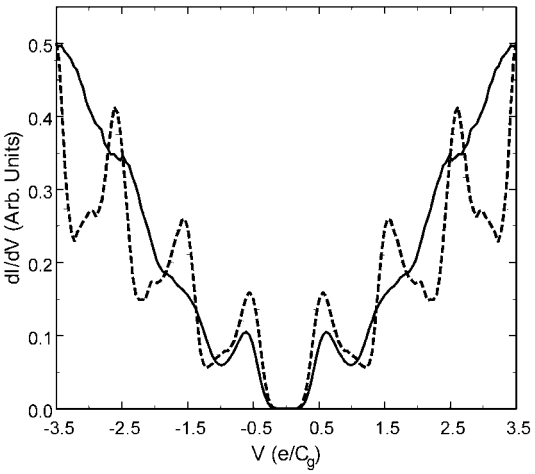


Fig. 3. The computed conductance of perfect chains (dashed curve) and disordered chains (solid curve) averaged over the angle between the chain axis and the electrode normal. For both curves, $T = 300$ K.

When core-size dispersion (±30 %) and orientation averaging are combined, the simulations still predict periodicity in the conductance, as shown by the solid curve in Figure 3. For these simulations 756 chains each having a different randomized set of capacitances and a different orientation were used. Interestingly, even with this degree of averaging, residual conductance periodicity is still found. While a direct comparison with the measured data (Fig. 1) cannot be made, it appears as if the amount of disorder used in the simulations overestimates the actual degree of disorder in the samples.

Finally, we address the nature of the current path and the fact that the measured voltage scale of the Coulomb blockade structure disagrees with the value determined from the capacitance. The conduction process must involve both the chains and the surface of the substrate. The origin of the surface conductance is likely a thin water layer, which is known to have ohmic behavior[30] and is expected given the wet chemical preparation method. The surface conductance is the background that is removed from the data (Fig. 1a, curve I) and is the means by which chains, arranged randomly on the surface, are electrically connected. Once the potential drop across a chain reaches the threshold value, the chain will come out of blockade and become part of the conduction path. Given that the chains are short compared to the inter-electrode spacing and that there does not appear to be a continuous path between the electrodes, the point at which a chain begins to conduct is a particular fraction of the applied voltage: that is, the surface conductance behaves in the manner of a potential divider which provides an explanation for the difference between the predicted and observed scales. It is known that the inter-particle spacing in ordered arrays of nanoparticles plays a key role in the nature of the electrical transport.[31,32] In the present samples the ligands provide a core separation that suggests electron hopping is the process responsible for charge transfer.[33] In this case, transport will be dominated through chains that have the lowest potential barriers between nanoparticles. Defects are expected to increase the potential barrier. Hence, chains that have the fewest missing or misplaced nanoparticles (defects) will govern the transport properties.

In summary, we have used a wet chemical process to produce extended nanoparticle arrays on biopolymer templates between electrode pairs. The *I–V* characteristics show clear evidence for single-electron charging effects in transport that is limited to one-dimension. From the computed capacitance values and numerical simulations we find that the chains likely contain between four and nine nanoparticles and that the *I–V* behavior of an ensemble of chains interconnected by the surface conduction of the substrate is tolerant toward variations of chain orientation, core size, and inter-particle spacing. Structure in the *I–V* characteristic is not robust toward variations in chain length, suggesting that a narrowly distributed range of chain lengths dominates the conduction in these samples. As a final point, we note that the measurements reported here used indirect electrical contact to an ensemble of nanoparticle arrays. This suggests that similar contact techniques, which avoid alignment between electrodes and nanoparticles, will be useful in their future electrical characterization and application.

Received: July 7, 2000
Final version: September 8, 2000

[1] G. Moore, in the 35th anniversary edition of *Electronics Magazine* **1965.**
[2] I. Amlani, A. O. Orlov, G. Toth, G. H. Bernstein, C. S. Lent, G. L. Snider, *Science* **1999**, *284*, 289.
[3] W. A. Schoonveld, J. Wildeman, D. Fichou, P. A. Bobbert, B. J. van Wees, T. M. Klapwijk, *Nature* **2000**, *404*, 977.
[4] D. V. Averin, K. K. Likharev, in *Mesoscopic Phenomena in Solids* (Eds: B. Al'tshuler, P. Lee, R. A. Webb), Elsevier, Amsterdam **1991**.
[5] N. Takahashi, H. Ishikuro, T. Hiramoto, *Appl. Phys. Lett.* **2000**, *76*, 209.
[6] T. W. Kim, S. O. Kang, D. C. Choo, J. H. Shim, *Appl. Phys. Lett.* **2000**, *76*, 1036.
[7] B. A Korgel, S. Fullam, S. Connolly, D. Fitzmaurice, *J. Phys. Chem. B* **1998**, *120*, 8379.
[8] R. P. Andres, J. D. Beielefeld, J. I. Henderson, D. B. Janes, V. R. Kolagunta, C. P. Kubiak, W. J. Mahoney, R. G. Osifchin, *Science* **1996**, *273*, 1690.
[9] R. P. Andres, T. Bein, M. Dorogi, S. Feng, J. I. Henderson, C. P. Kubiak, W. Mahoney, R. G. Osifchin, R. Reifenberger, *Science* **1996**, *272*, 1323.
[10] S. Datta, W. Tian, S. Hong, R. Reifenberger, J. I. Henderson, C. P. Kubiak, *Phys. Rev. Lett.* **1997**, *79*, 2530.
[11] D. L. Feldheim, K. C. Grabar, M. J. Natan, T. E. Mallouk, *J. Am. Chem. Soc.* **1996**, *118*, 7640.
[12] J. R. Heath, P. J. Kuekes, G. S. Snider, R. S. Williams, *Science* **1998**, *280*, 1716.
[13] C. P. Collier, E. W. Wong, M. Belohradský, F. M. Raymo, J. F. Stoddart, P. J. Kuekes, R. S. Williams, J. R. Heath, *Science* **1999**, *285*, 391.
[14] E. Braun, Y. Eichen, U. Sivan, G. Ben-Yoseph, *Nature* **1998**, *391*, 775.
[15] T. Sato, H. Ahmed, D. Brown, B. F. G. Johnson, *J. Appl. Phys.* **1997**, *82*, 696.
[16] S. H. Magnus Persson, L. Olofsson, L. Gunnarsson, *Appl. Phys. Lett.* **1999**, *74*, 2546.
[17] K. Kawaski, M. Mochizuki, K. Tsutsui, *Jpn. J. Appl. Phys.* **1999**, *38*, 418.
[18] M. N. Wybourne, J. E. Hutchison, L. Clarke, L. O. Brown, J. L. Mooster, *Microelectron. Eng.* **1999**, *47*, 55.
[19] The samples were prepared as follows. First, a $2.2 \times 10^{-5}$ mol/L solution of PLL–hydrobromide complex (54 000 amu) in 10/90 % water/methanol was drop cast onto the electrodes that had been pre-cleaned using a UV/ozone dry process followed by a rinse in nanopure water. The hydrobromide was removed from the amine side chains of the biopolymer by submerging the cast film in a solution of 1 % sodium hydroxide in water for about 20 h. The 11-mercaptoundecanoic acid stabilized gold nanoparticles were synthesized from Schmid-$Au_{55}$ nanoparticles (G. Schmid, *Inorg. Synth.* **1990**, *27*, 214) using ligand exchange (L. O. Brown, J. E. Hutchison, *J. Am. Chem. Soc.* **1997**, *119*, 12 384). Nanoparticle decoration of the bio-

  0935-9648/01/0201-0112 $ 17.50+.50/0 

polymer was accomplished by placing a concentrated solution of the nanoparticles in dimethylsulfoxide onto the PLL film for about 20 min, after which it was rinsed in dimethylsulfoxide and then dichloromethane. From the molecular weight, the average length of the PLL is about 30 nm. Therefore, each polymer can accommodate about seven or eight nanoparticles.

[20] L. Clarke, M. N. Wybourne, M. Yan, S. X. Cai, J. F. W. Keana, *Appl. Phys. Lett.* **1997**, *71*, 617.
[21] A. A. Middleton, N. S. Wingreen, *Phys. Rev. Lett.* **1993**, *71*, 3198.
[22] G. Y. Hu, R. F. O'Connell, *Phys. Rev. B* **1994**, *49*, 16 773.
[23] A. J. Rimberg, T. R. Ho, J. Clarke, *Phys. Rev. Lett.* **1995**, *74*, 4714.
[24] L. Clarke, M. N. Wybourne, M. Yan, S. X. Cai, L. O. Brown, J. Hutchison, J. F. W. Keana, *J. Vac. Sci. Technol. B* **1997**, *15*, 2925.
[25] The capacitance matrix was calculated for different chain lengths using the software package FastCap MIT (**1992**). We used the nanoparticle dimensions given in the text and a ligand shell dielectric constant of 3. For nanoclusters away from the end of the chains we obtain $C_{dd} \approx 0.04$ aF and $C_g \approx 0.17$ aF. As expected, the value of $C_g$ is slightly larger than the value calculated for an isolated metal sphere of radius $a$ coated with a dielectric shell, $C_g \approx (4\pi\varepsilon\varepsilon_0 a)/(1 + (a/d)(\varepsilon - 1)) = 0.14$ aF, where $d$ is the total radius of the core plus ligand shell.
[26] Simulations were carried out using both MOSES (Monte-Carlo Single-Electronics Simulator, R. H. Chen) and SIMON (Simulation of Nano Structures, C. Wasshuber).
[27] S. Chen, R. S. Ingram, M. J. Hostetler, J. J. Pietron, R. W. Murray, T. G. Schaaff, J. T. Khoury, M. M. Alvarez, R. L. Whetton, *Science* **1998**, *280*, 2098.
[28] L. Y. Gorelik, A. Isacsson, M. V. Voinova, B. Kasemo, R. I. Shekhter, M. Jonson, *Phys. Rev. Lett.* **1998**, *80*, 4526.
[29] O. D. Häberlen, S. C. Chung, M. Stener, N. Rösch, *J. Chem. Phys.* **1997**, *106*, 5189.
[30] Y. Awakuni, J. H. Calderwood, *J. Phys. D: Appl. Phys.* **1972**, *5*, 1038.
[31] G. Markovich, C. P. Collier, J. R. Heath, *Phys. Rev. Lett.* **1998**, *80*, 3807.
[32] C. P. Collier, R. J. Saykally, J. J. Shiang, S. E. Hendrichs, J. R. Heath, *Science* **1997**, *277*, 1978.
[33] N. Mott, *Metal Insulator Transitions*, Taylor and Francis, London **1990**.

## Catalytic Growth of Zinc Oxide Nanowires by Vapor Transport**

By *Michael H. Huang*, *Yiying Wu*, *Henning Feick*, *Ngan Tran*, *Eicke Weber*, and *Peidong Yang**

Recent progress in the synthesis and characterization of nanowires has been driven by the need to understand the novel physical properties of one-dimensional nanoscale materials, and their potential application in constructing nanoscale electronic and optoelectronic devices.[1] Nanowires with different compositions have been explored using various methods including the vapor-phase transport process,[2–4] chemical vapor deposition,[5] arc discharge,[6] laser ablation,[7] solution,[8,9] and a template-based method.[10,11] While a large part of this work has been focused on semiconductor systems such as Si,[1] Ge,[2] GaN,[3,10] GaAs,[5,7] only a few studies on oxide systems exist in the literature. Among them, MgO nanowires have been synthesized and incorporated into high-temperature superconductors to improve the critical current densities of the superconductors.[12,13] Several other oxide nanowires, including $SiO_2$,[14] $GeO_2$,[4] and $Ga_2O_3$,[6] have also been reported although the insulating nature of these oxide systems could limit, if any, their applications. It is thus necessary to look into other oxide systems with interesting optical, electrical, and magnetic properties.

ZnO, a wide bandgap (3.37 eV) semiconductor with large exciton binding energy (60 meV), has been investigated as a short-wavelength light-emitting, transparent conducting and piezoelectric material. ZnO nanoclusters and thin films have also been shown to exhibit room temperature UV lasing properties.[15] Most of the ZnO nanomaterials studied are in the form of nanoparticles although needle crystals and large whiskers have been previously reported.[16] Polycrystalline ZnO nanowires have also been recently fabricated within a porous alumina template.[11] Due to the promising application of ZnO nanowires in nanoscale optoelectronic devices, it is important to be able to synthesize these nanowires in single-crystalline form and study their optical properties. Here we report the use of the vapor-phase transport process to grow ZnO nanowires via the vapor–liquid–solid (VLS) mechanism. The Zn vapor is generated using carbothermal or hydrogen reduction of ZnO. Size control of the nanowire diameters was achieved by varying the thickness of the thin film Au catalyst. It is also possible to grow thinner wires by using monodispersed Au colloids dispersed on substrates as catalysts. In addition, a ZnO nanowire network has been successfully synthesized on patterned Au catalysts. Photoluminescence (PL) characterization of the nanowires shows that these nanowires exhibit strong UV emission and size-dependent green light emission.

ZnO nanowires were grown on Au-coated silicon substrates by heating a 1:1 mixture of ZnO and graphite powder to 900–925 °C under a constant flow of argon for 5–30 min. The substrate surface appeared light or dark gray after the reaction, indicating the deposition of material. X-ray diffraction (XRD) patterns of ZnO nanowire samples were taken to examine the crystal structure of the nanowires. All samples gave similar XRD patterns indicating the nanowires' high crystallinity. Figure 1 shows a typical XRD pattern of the ZnO nanowires. The diffraction peaks can be indexed to a hexagonal structure of bulk ZnO with cell constants of $a$ = 3.24 and $c$ = 5.19 Å. While Au (111) and (200) peaks have been detected in some samples, no diffraction peaks from Zn have been found in any of our samples.

The morphology of the materials on the substrate was examined by scanning electron microscopy (SEM). A typical SEM image for nanowires grown on a substrate coated with

[*] Prof. P. Yang, Dr. M. H. Huang, Y. Wu, N. Tran
Department of Chemistry, University of California
Berkeley, CA 94720 (USA)
E-mail: pyang@cchem.berkeley.edu
Prof. E. Weber, Dr. H. Feick
Department of Materials Science and Engineering
Materials Science Division, Lawrence Berkeley National Laboratory
University of California
Berkeley, CA 94720 (USA)

[**] This work was supported by the Camille and Henry Dreyfus Foundation, 3M Corporation, and University of California, Berkeley. Work at the Lawrence Berkeley National Laboratory was supported by the Office of Science, Basic Energy Sciences, Division of Materials Science, of the U.S. Department of Energy under contract No. DE-AC03-76SF00098. We thank Vojislav Srdanov at University of California, Santa Barbara for help during the power-dependent emission measurement. We thank the Microfabrication Laboratories and the National Center for Electron Microscopy for the use of their facilities.

  0935-9648/01/0201-0113 $ 17.50+.50/0 